Inorg. Chem. **2007**, *46*, 5110–5117

Dinitrosyl Iron Complexes (DNICs) Containing S/N/O Ligation: Transformation of Roussin's Red Ester into the Neutral $\{Fe(NO)_2\}^{10}$ DNICs

Ming-Li Tsai, Chung-Hung Hsieh, and Wen-Feng Liaw*

Department of Chemistry, National Tsing Hua University, Hsinchu 30013, Taiwan

Received February 9, 2007

Addition of the Lewis base $[OPh]^-$ to the THF solution of Roussin's red ester $[Fe(\mu\text{-}SC_6H_4\text{-}o\text{-}NHCOPh)(NO)_2]_2$ (**1**) and $[Fe(\mu\text{-}SC_6H_4\text{-}o\text{-}COOH)(NO)_2]_2$ (**2**), respectively, yielded the EPR-active, anionic $\{Fe(NO)_2\}^9$, $[(SC_6H_4\text{-}o\text{-}NCOPh)\text{-}Fe(NO)_2]^-$ (**3**) with the anionic $[SC_6H_4\text{-}o\text{-}NCOPh]^{2-}$ ligand bound to the $\{Fe(NO)_2\}$ core in a bidentate manner (S,N-bonded) and $[(SC_6H_4\text{-}o\text{-}COO)Fe(NO)_2]^-$ (**4**) with the anionic $[SC_6H_4\text{-}o\text{-}COO]^{2-}$ ligand bound to the $\{Fe(NO)_2\}$ core in a bidentate manner (S,O-bonded), characterized by IR, UV–vis, EPR, and single-crystal X-ray diffraction. In contrast to the bridged-thiolate cleavage yielding the neutral $\{Fe(NO)_2\}^9$, $[(SC_6H_4\text{-}o\text{-}NHCOPh)(Im)Fe(NO)_2]$ (Im = imidazole), by addition of 2 equiv of imidazole to complex **1** observed in the previous study, the addition of the stronger σ-donating and π-accepting PPh_3 ligand triggered the reductive elimination of bridged thiolates of complex **1** to yield the neutral $\{Fe(NO)_2\}^{10}$, $[(PPh_3)_2Fe(NO)_2]$. These results unambiguously illustrate one aspect of how the nucleophile L (L = imidazole, PPh_3, $[OPh]^-$) functions to control the reaction pathways (bridged-thiolate cleavage, reductive elimination, and deprotonation) upon the reaction of complex **1** and the nucleophile L. The EPR-active, dimeric $\{Fe(NO)_2\}^9$ dinitrosyl iron complex (DNIC) $[Fe(\mu\text{-}SC_7H_4SN)(NO)_2]_2$ (**6**), with S and N atoms of the anionic $[\text{–}SC_7H_4SN\text{–}]^-$ (2-benzothiozolyl thiolate) ligands bound to two separate $\{Fe(NO)_2\}^9$ cores, was also synthesized from reaction of bis(2-benzothiozolyl) disulfide and $[(NO)_2Fe(PPh_3)_2]$. A straightforward reaction of complex **6** and 4 equiv of $[N_3]^-$ conducted in THF led to the anionic $\{Fe(NO)_2\}^9$, $[(N_3)_2Fe(NO)_2]^-$ (**7**). Conclusively, the EPR-active, $\{Fe(NO)_2\}^9$ DNICs can be classified into the anionic $\{Fe(NO)_2\}^9$ DNICs with S/N/O ligation, the neutral $\{Fe(NO)_2\}^9$ DNIC with one thiolate and one neutral imidazole ligation, and the cationic $\{Fe(NO)_2\}^9$ DNICs with the neutral N-/P-containing coordinated ligands.

Introduction

Dinitrosyl iron complexes (DNICs) have been known to be one of two possible forms for storage and transport of NO in biological systems.[1] Formation of dinitrosyl iron complexes (DNICs) and dinuclear $[Fe(\mu\text{-}SR)(NO)_2]_2$ (Roussin's red ester) by nitrosylation of iron−sulfur cluster-containing proteins in mitochondria and reactions of nitric oxide with thiol-rich proteins in the presence of free iron have been intensely studied.[1−3] Characterization of both protein-bound and low-molecular weight DNICs (LMW-DNICs) in vitro has been made possible via their distinctive EPR signals at $g = 2.03$.[1−5] Although cysteine and glu-

* To whom correspondence should be addressed. E-mail: wfliaw@mx.nthu.edu.tw.

(1) (a) Stamler, J. S. *Cell* **1994**, *78*, 931−936. (b) Stamler, J. S.; Singel, D. J.; Loscalzo, J. *Science* **1992**, *258*, 1898−1902. (c) Ford, P. C.; Lorkovic, I. M. *Chem. Rev.* **2002**, *102*, 993−1017. (d) Hayton, T. W.; Legzdins, P.; Sharp, W. B. *Chem. Rev.* **2002**, *102*, 935−991. (e) Butler, A. R.; Megson, I. L. *Chem. Rev.* **2002**, *102*, 1155−1165. (f) Ueno, T.; Susuki, Y.; Fujii, S.; Vanin, A. F.; Yoshimura, T. *Biochem. Pharmacol.* **2002**, *63*, 485−493. (g) Lee, J.; Chen, L.; West, A. H.; Richter-Addo, G. B. *Chem. Rev.* **2002**, *102*, 1019−1065. (h) McCleverty, J. A. *Chem. Rev.* **2004**, *104*, 403−418.

(2) (a) Foster, M. W.; Cowan, J. A. *J. Am. Chem. Soc.* **1999**, *121*, 4093−4100. (b) Ding, H.; Demple, B. *Proc. Natl. Acad. Sci. U.S.A.* **2000**, *97*, 5146−5150.

(3) (a) Cesareo, E.; Parker, L. J.; Parker, L. J.; Pedersen, J. Z.; Nuccetelli, M.; Mazzetti, A. P.; Pastore, A.; Federici, G.; Caccuri, A. M.; Ricci, G.; Adams, J. J.; Parker, M. W.; Bello, M. L. *J. Biol. Chem.* **2005**, *280*, 42172−42180. (b) Maria, F. D.; Pedersen, J. Z.; Caccuri, A. M.; Antonini, G.; Turella, P.; Stella, L.; Bello, M. L.; Federici, G.; Ricci, G. *J. Biol. Chem.* **2003**, *278*, 42283−42293. (c) Lancaster, J. R., Jr.; Hibbs, Jr. J. B. *Proc. Natl. Acad. Sci. U.S.A.* **1990**, *87*, 1223−1227.

(4) (a) Boese, M.; Mordvintcev, P. I.; Vanin, A. F.; Busse, R.; Mülsch, A. *J. Biol. Chem.* **1995**, *270*, 29244−29249. (b) Lee, M.; Arosio, P.; Cozzi, A.; Chasteen, M. D. *Biochemistry* **1994**, *33*, 3679−3687. (c) Branca, M.; Culeddu, N.; Fruianu, M.; Marchettini, N.; Tiezzi, E. *Magn. Reson. Chem.* **1997**, *35*, 687−690. (d) Lewandowska, H.; Meczyńska, S.; Sochanowicz, B.; Sadlo, J.; Kruszewski, M. *J. Biol. Inorg. Chem.* **2007**, *12*, 345−352.

10.1021/ic0702567 CCC: $37.00
Published on Web 04/20/2007

Table 1. List of the Reported Protein-Bound DNICs Based on EPR Spectra

name	coordination environment	EPR	ref
bovine serum albumin	S/S	2.01, 2.04	4a
	S/N	2.01, 2.04, 2.05	
	N/N	2.01, 2.35, 2.055	
Sox R	S/S	2.03	2b
mammalian ferrochelatase	S/S	2.014, 2.033	5a
aconitase	S/S	2.012, 2.031, 2.037	5b
	N/N	2.004, 2.034, 2.016	
FNR	S/S	2.016, 2.034, 2.038	5c
succinate-Q reductase	S/S	2.04	5d
GST P1-1	S/O	2.015, 2.028, 2.038	3
mammalian ferritin	S/S	2.014, 2.033	4b
	N/N	2.015, 2.033, 2.055	
Fur	N or O	2.017, 2.032, 2.042	5e
	N or O	silent	
iron−quinone complex of photosystem II	N/N	2.01, 2.03, 2.05	5f

tathione have been proposed to be the major thiol components of cellular DNICs in vivo,[4d] three different kinds of potential coordinated ligands (thiolate, amine, and alkoxide) in DNICs were found and proposed in enzymology (Table 1).[2b,3,4a,4b,5] In particular, the protein-bound DNICs have been well characterized by X-ray crystallography through interaction of human glutathione transferase P1-1 and dinitrosyl diglutathionyl iron complex in vitro/in vivo.[3] Also, amine-coordinated DNICs are found as the intermediate of albumin, Fur-Fe, and iron-quinone complexes via nitrosylation.[4a]

On the basis of oxidation levels of the $\{Fe(NO)_2\}$ core of DNICs, the known stable LMW-DNICs can be classified into the EPR-active, anionic $\{Fe(NO)_2\}^9$ neutral $\{Fe(NO)_2\}^9$ and cationic $\{Fe(NO)_2\}^9$ DNICs, and the EPR-silent, neutral $\{Fe(NO)_2\}^{10}$ DNICs in inorganic chemistry.[6−7] Here, the electronic state of the $\{Fe(NO)_2\}$ unit of DNICs is generally designated as $\{Fe(NO)_2\}^n$. This formalism $\{M(NO)_2\}^n$ (M = transition metal), in which n is the total number of electrons associated with the metal d and π^*(NO) orbitals, follows the Enemark−Feltham notation which stresses the well-known covalence and delocalization in the $M(NO)_2$ unit.[8] In spite of a large number of mononuclear $\{Fe(NO)_2\}^9$ dinitrosyl iron complexes,[6−7] examples of the mononuclear $\{Fe(NO)_2\}^9$ dinitrosyl iron complexes containing S/N/O ligation are limited.[3,6,7]

Recently, we have shown that the facile transformation of the neutral $\{Fe(NO)_2\}^{10}$, [(sparteine)$Fe(NO)_2$], to the anionic $\{Fe(NO)_2\}^9$, $[(S(CH_2)_3S)Fe(NO)_2]^-$, may occur via the cationic $\{Fe(NO)_2\}^9$, $[(sparteine)Fe(NO)_2]^+$. Here, the complex $[(sparteine)Fe(NO)_2]^+$ acts as an $\{Fe(NO)_2\}$-donor reagent in the presence of $[S(CH_2)_3S]^{2-}$.[7d] The transformation of Roussin's red ester $[Fe(\mu\text{-}SC_6H_4\text{-}o\text{-}NHCOPh)(NO)_2]_2$ into the neutral $\{Fe(NO)_2\}^9$, $[(SC_6H_4\text{-}o\text{-}NHCOPh)(Im)Fe(NO)_2]$ (Im = imidazole), was demonstrated by reaction of $[Fe(\mu\text{-}SC_6H_4\text{-}o\text{-}NHCOPh)(NO)_2]_2$ with imidazole.[7c] Ligand-replacement between the neutral $\{Fe(NO)_2\}^9$, $[(SC_6H_4\text{-}o\text{-}NHCOPh)(Im)Fe(NO)_2]$, and the thiolate $[SC_6H_4\text{-}o\text{-}NHCOPh]^-$ led to the formation of the anionic $\{Fe(NO)_2\}^9$, $[(SC_6H_4\text{-}o\text{-}NHCOPh)_2Fe(NO)_2]^-$. In the study of dinuclear DNICs, the diamagnetic dinuclear iron−thiolate complex $[(ON)Fe(S,S\text{-}C_6H_4)_2Fe(NO)_2]^-$ containing a $\{Fe(NO)_2\}^9$ dinitrosyl iron motif stabilized by $\{Fe(NO)\}^7$−$\{Fe(NO)_2\}^9$ coupling was synthesized and characterized.[9] The objective of this study was to delineate the synthesis and reactivity of the EPR-active, anionic $\{Fe(NO)_2\}^9$, $[(SC_6H_4\text{-}o\text{-}NCOPh)Fe(NO)_2]^-$ (**3**), $[(SC_6H_4\text{-}o\text{-}COO)Fe(NO)_2]^-$ (**4**), and $[(N_3)_2Fe(NO)_2]^-$ (**7**), containing a wide range of S/N/O ligation and the EPR-active, dimeric $\{Fe(NO)_2\}^9$−$\{Fe(NO)_2\}^9$ DNICs $[Fe(\mu\text{-}SC_7H_4SN)(NO)_2]_2$ (**6**). Specifically, the transformation of Roussin's red esters (RREs) $[Fe(\mu\text{-}SC_6H_4\text{-}o\text{-}NHCOPh)(NO)_2]_2$ (**1**) and $[Fe(\mu\text{-}SC_6H_4\text{-}o\text{-}COOH)(NO)_2]_2$ (**2**) into (i) the neutral $\{Fe(NO)_2\}^{10}$, $[(PPh_3)_2Fe(NO)_2]$, via reductive elimination of the bridged thiolates, and (ii) the anionic $\{Fe(NO)_2\}^9$ DNICs **3** and **4** incorporating anionic sulfur−amide and sulfur−carboxylate chelates, respectively, controlled by the nucleophile L (L = PPh_3, $[OPh]^-$), were elucidated through reaction of Roussin's red esters **1** and **2** with the nucleophile L.

Results and Discussion

As has been known, reaction of diaryl disulfides $(RS)_2$ (R = C_6H_4-*o*-NHCOPh, C_6H_4-*o*-COOH) (0.1 mmol) and $Fe(CO)_2(NO)_2$ (0.2 mmol)[9,10] in tetrahydrofuran (THF) at ambient temperature yielded Roussin's red esters $[Fe(\mu\text{-}SR)(NO)_2]_2$ (R = C_6H_4-*o*-NHCOPh (**1**), C_6H_4-*o*-COOH (**2**)) isolated as a brown-green solid (Scheme 1a).[7c,11] Complexes **1** and **2** exhibited diagnostic IR ν_{NO} stretching frequencies at 1758 s, 1786 s, 1816 vw, and 1756 s, 1782 s, 1812 vw cm^{-1} (THF), respectively. Consistent with other Roussin's red esters,[7c,11] complexes **1** and **2** were best described as the dimeric dinitrosyl iron complexes with $\{Fe(NO)_2\}^9$−$\{Fe(NO)_2\}^9$ coupling. Both Fe centers ($S = {}^1/_2$) magnetically

(5) (a) Sellers, V. M.; Johnson, M. K.; Dailey, H. A. *Biochemistry* **1996**, *35*, 2699−2704. (b) Kennedy, M. C.; Antholine, W. E.; Beinert, H. *J. Biol. Chem.* **1997**, *272*, 20340−20347. (c) Cruz-Ramos, H.; Crack, J.; Wu, G.; Hughes, M. N.; Scott, C.; Thomson, A. J.; Green, J.; Poole, R. K. *EMBO J.* **2002**, *21*, 3235−3244. (d) Welter, R.; Yu, L.; Yu, C.-A. *Arch. Biochem. Biophys.* **1996**, *331*, 9−14. (e) D'Autréaux, B.; Horner, O.; Oddou, J.-L.; Jeandey, C.; Gambarelli, S.; Berthomieu, C.; Latour, J.-M.; Michaud-Soret, I. *J. Am. Chem. Soc.* **2004**, *126*, 6005−6016. (f) Goussias, C.; Deligiannakis, Y.; Sanakis, Y.; Ioannidis, N.; Petrouleas, V. *Biochemistry* **2002**, *41*, 15212−15223.

(6) (a) Chiang, C.-Y.; Miller, M. L.; Reibenspies, J. H.; Darensbourg, M. Y. *J. Am. Chem. Soc.* **2004**, *126*, 10867−10874. (b) Baltusis, L. M.; Karlin, K. D.; Rabinowitz, H. N.; Dewan, J. C.; Lippard, S. J. *Inorg. Chem.* **1980**, *19*, 2627−2632. (c) Reginato, N.; McCrory, C. T. C.; Pervitsky, D.; Li, L. *J. Am. Chem. Soc.* **1999**, *121*, 10217−10218. (d) Butler, A. R.; Glidewell, C.; Li, M.-H. *Adv. Inorg. Chem.* **1988**, *32*, 335−393.

(7) (a) Tsai, M.-L.; Chen, C.-C.; Hsu, I.-J.; Ke, S.-C.; Hsieh, C.-H.; Chiang, K.-A.; Lee, G.-H.; Wang, Y.; Liaw, W.-F. *Inorg. Chem.* **2004**, *43*, 5159−5167. (b) Tsai, F.-T.; Chiou, S.-J.; Tsai, M.-C.; Tsai, M.-L.; Huang, H.-W.; Chiang, M.-H.; Liaw, W.-F. *Inorg. Chem.* **2005**, *44*, 5872−5881. (c) Tsai, M.-L.; Liaw, W.-F. *Inorg. Chem.* **2006**, *45*, 6583−6585. (d) Hung, M.-C.; Tsai, M.-C.; Lee, G.-H.; Liaw, W.-F. *Inorg. Chem.* **2006**, *45*, 6041−6047. (e) Lu, T.-T.; Chiou, S.-J.; Chen, C.-Y.; Liaw, W.-F. *Inorg. Chem.* **2006**, *45*, 8799−8806. (f) Chen, T.-N.; Lo, F.-C.; Tsai, M.-L.; Shih, K.-N.; Chiang, M.-H.; Lee, G.-H.; Liaw, W.-F. *Inorg. Chim. Acta* **2006**, *359*, 2525−2533.

(8) Enemark, J. H.; Feltham, R. D. *Coord. Chem. Rev.* **1974**, *13*, 339−406.

(9) Chen, H.-W.; Lin, C.-W.; Chen, C.-C.; Yang, L.-B.; Chiang, M.-H.; Liaw, W.-F. *Inorg. Chem.* **2005**, *44*, 3226−3232.

(10) Albano, V. G; Araneo, A; Bellon, P. L.; Ciani, G.; Manassero, M. *J. Organomet. Chem.* **1974**, *67*, 413−422.

(11) Rauchfuss, T. B.; Weatherill, T. D. *Inorg. Chem.* **1982**, *21*, 827−830.

Scheme 1

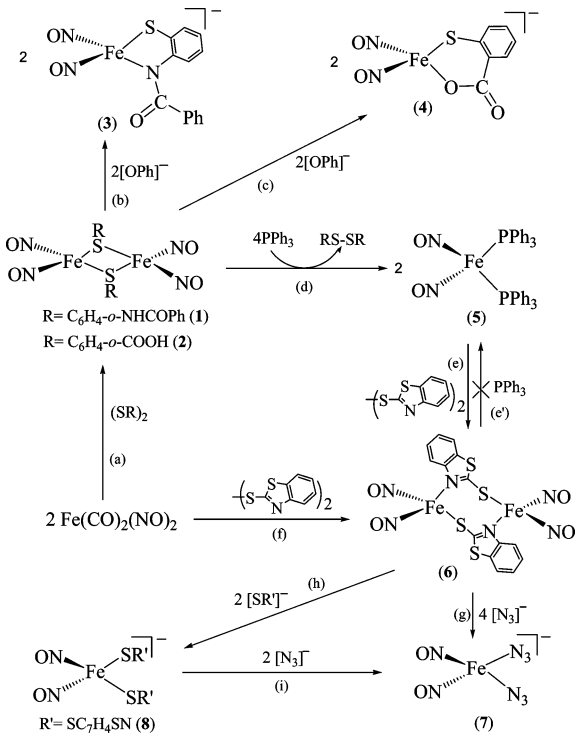

couple to each other via the mediation of thiolate bridges, which rationalizes the absence of paramagnetism and the EPR signal.[9]

As presented in Scheme 1b, upon addition of 2 equiv of $[OPh]^-$ into a THF solution of complex **1** at ambient temperature, instead of the formation of the anionic $\{Fe(NO)_2\}^9$, $[(OPh)(SC_6H_4\text{-}o\text{-}NHCOPh)Fe(NO)_2]^-$, via splitting of the thiolate bridges, a reaction ensued over the course of 5 min to yield the dark-purple $[(SC_6H_4\text{-}o\text{-}NCOPh)Fe(NO)_2]^-$ (**3**) with the dianionic $[SC_6H_4\text{-}o\text{-}NCOPh]^{2-}$ ligand bound to the $\{Fe(NO)_2\}$ core in a bidentate manner (S,N-bonded) identified by single-crystal X-ray diffraction. The shift in IR ν(NO) from 1758 s, 1786 s, 1816 vw cm^{-1} (complex **1**) to 1690 s, 1737 s cm^{-1} (THF) is in accordance with the formation of the anionic $\{Fe(NO)_2\}^9$ DNIC **3** (yield 63%).[7] The EPR spectrum of complex **3** exhibits an isotropic signal with $g = 2.034$ at 298 K and a rhombic signal with $g_1 = 2.052$, $g_2 = 2.033$, and $g_3 = 2.011$ at 77 K (Figure 1a), the characteristic g value of the $\{Fe(NO)_2\}^9$ DNICs.[6,7] In contrast to the bridged-thiolate cleavage observed in the reaction of complex **1** and imidazole,[7c] the formation process was best assigned to the deprotonation of the bridged-thiolate $[SC_6H_4\text{-}o\text{-}NHCOPh]$ of complex **1**, and the subsequent chelation of the dianionic ligand $[SC_6H_4\text{-}o\text{-}NCOPh]^{2-}$ leading to the formation of complex **3**. The surprisingly stable complex **3** is the first example of the anionic $\{Fe(NO)_2\}^9$ DNICs containing the chelating 2-thiolatophenylamido (S,N-coordinated) coordinated to the $\{Fe(NO)_2\}^9$ motif isolated and characterized by single-crystal X-ray diffraction.

In a similar fashion, upon addition of 2 equiv of $[OPh]^-$ to the THF solution of complex **2**, a pronounced color change from brown to dark-brown occurs at ambient temperature. The IR, UV−vis, EPR, and X-ray diffraction studies confirmed the formation of the anionic $\{Fe(NO)_2\}^9$, $[(SC_6H_4\text{-}o\text{-}COO)Fe(NO)_2]^-$ (**4**) (yield 0.077 g, 93%), with the dianionic $[SC_6H_4\text{-}o\text{-}COO]^{2-}$ ligand bound to the $\{Fe(NO)_2\}$ core in a bidentate manner (S,O-bonded) (Scheme 1c).[3a] As observed in the transformation of complex **1** to **3**, the conversion of complex **2** to complex **4** is presumed to occur via deprotonation of the bridged-thiolate $[SC_6H_4\text{-}o\text{-}COOH]^-$ and the subsequent chelation of $[SC_6H_4\text{-}o\text{-}COO]^{2-}$ ligand. The EPR spectrum of complex **4** exhibits an isotropic signal with $g = 2.034$ at 298 K and high rhombicities with three principal g values of 2.054, 2.036, and 2.012 at 77 K (Figure 1b), the characteristic g values of the $\{Fe(NO)_2\}^9$ DNICs.[7] The conversion of complex **2** to **4** was also monitored by UV−vis spectrometry; the intense bands at 387 and 792 nm disappeared accompanied by the simultaneous formation of the absorption bands at 475 and 947 nm. We noticed that the IR spectra for the anionic complex **3** and complex **4** had the same pattern but differed in position (1690, 1737 cm^{-1} for **3** vs 1688, 1742 cm^{-1} for **4** (THF)) and separation of NO stretching frequencies ($\Delta\nu_{NO}$) ($\Delta\nu_{NO} = 47$ cm^{-1} for **3** vs 54 cm^{-1} for **4**).

In contrast to the deprotonation of bridged thiolates yielding complexes **3** and **4** observed in the reaction of complexes **1** and **2** and $[OPh]^-$, respectively, and the bridged-thiolate cleavage yielding the neutral $\{Fe(NO)_2\}^9$, $[(SC_6H_4\text{-}o\text{-}NHCOPh)(imidazole)Fe(NO)_2]$, observed in the reaction of complex **1** and imidazole,[7c] the addition of 4 equiv of PPh_3 to complex **1** in THF at ambient temperature led to the formation of the known neutral $\{Fe(NO)_2\}$,[10] $[(PPh_3)_2Fe(NO)_2]$ (**5**), identified by IR and UV−vis spectra (Supporting Information Figure S1),[10b,10c] and $(SC_6H_4\text{-}o\text{-}NHCOPh)_2$ characterized by IR and ^1H NMR spectra (Scheme 1d). The conversion of complex **1** to complex **5** was also monitored by UV−vis spectrometry; the bands at 438 and 789 nm disappeared with concomitant formation of a spectrum (the absorption bands at 445 and 665 nm) in accordance with the formation of the EPR-silent complex **5**. Many attempts by monitoring the FTIR spectrum of the reaction in THF to detect the possible intermediate $[(SC_6H_4\text{-}o\text{-}NHCOPh)(PPh_3)Fe(NO)_2]$ were unsuccessful. Presumably, the stronger σ-donor and π-acceptor PPh_3 ligands trigger the reductive elimination of the bridged-thiolate ligands of complex **1** and result in the transformation of complex **1** into the neutral $\{Fe(NO)_2\}^{10}$ DNIC **5**.

As presented in Scheme 1e,f, upon addition of complex **5** (or $[Fe(CO)_2(NO)_2]$) into a THF solution of bis(2-benzothiozolyl) disulfide ($(SC_7H_4SN)_2$) in a 2:1 stoichiometry, a reaction ensued over the course of 5 min to yield the neutral, EPR-active, dimeric DNIC $[Fe(\mu\text{-}SC_7H_4SN)(NO)_2]_2$ (**6**) with S and N atoms of the bridging $[-SC_7H_4SN-]^-$ ligands bound to two separate $\{Fe(NO)_2\}$ cores, respectively. The dinuclear $\{Fe(NO)_2\}^9$−$\{Fe(NO)_2\}^9$ DNIC **6** was characterized by IR, EPR, UV−vis, and single-crystal X-ray diffraction. In contrast to the EPR-silent complexes **1** and **2**, the EPR spectrum of complex **6** exhibits a rhombic signal ($g =$ 2.042, 2.033, and 2.013) (an isotropic signal with $g = 2.033$ at 298 K) (Figure 2a) and a weak half-field signal at $g =$

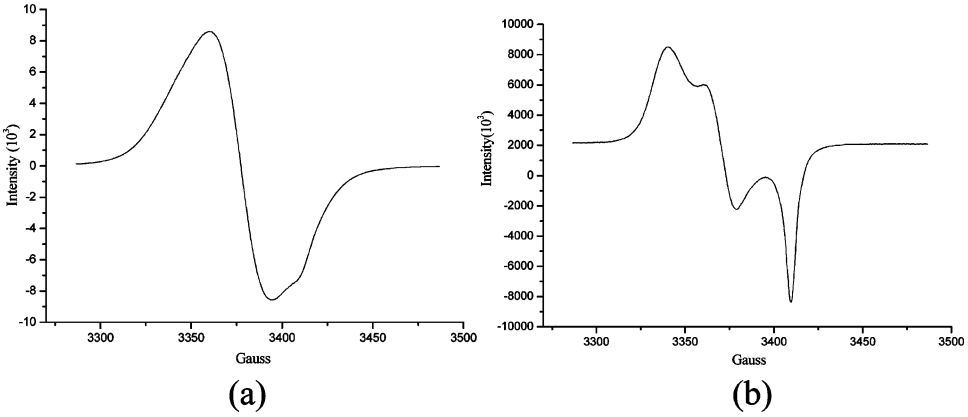

Figure 1. (a) EPR spectrum of complex **3** with $g_1 = 2.052$, $g_2 = 2.033$, and $g_3 = 2.011$; $A_1 = 30$ G, $A_2 = 20$ G, and $A_3 = 28$ G (isotropic, $g_{av} = 2.034$ at 298 K) at 77 K. (b) EPR spectrum of complex **4** with $g_1 = 2.054$, $g_2 = 2.036$, $g_3 = 2.012$; $A_1 = 13$ G, $A_2 = 16$ G, and $A_3 = 8$ G (isotropic, $g_{av} = 2.034$ at 298 K) at 77 K.

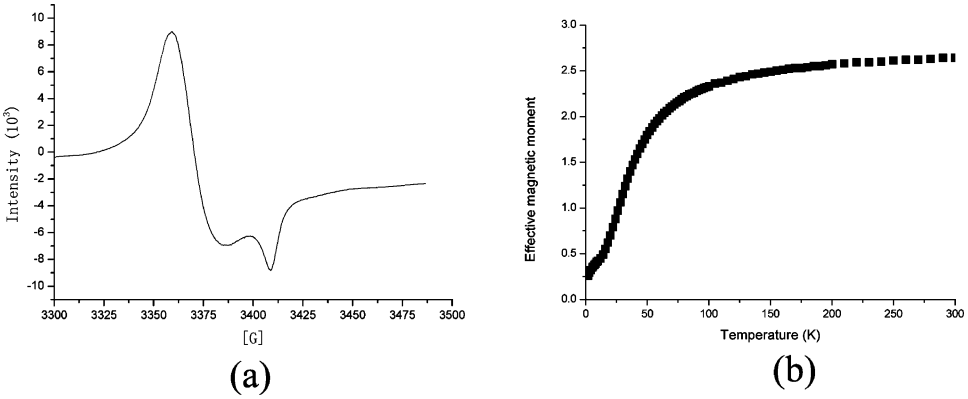

Figure 2. (a) EPR spectrum of complex **6** with $g = 2.042$, 2.033, and 2.013 ($A_1 = 18$ G, $A_2 = 18$ G, and $A_3 = 14$ G) at 77 K (isotropic, $g_{av} = 2.033$ at 298 K). (b) Plot of effective magnetic moment (μ_B) vs temperature for complex **6**.

4.05 at 77 K (Supporting Information Figure S2).[12] The weak magnetic coupling (dipolar coupling) between the two $\{Fe(NO)_2\}^9$ centers ($S = {}^1/_2$) resulting from the long Fe···Fe distance (3.997 Å) rationalizes the presence of the EPR half-field signal in complex **6**.[12] As shown in Figure 2b, the temperature-dependent effective magnetic moment in solid state by SQUID magnetometer decreases from 2.64 μ_B at 300 K to 1.80 μ_B at 50 K, consistent with the dimeric $\{Fe(NO)_2\}^9$–$\{Fe(NO)_2\}^9$ electronic configuration containing weak dipolar coupling in complex **6**. We noticed that the IR spectra for the neutral complexes **1** and **2** and the neutral dimeric DNIC **6** had the different pattern and position (1816 vw, 1786 s, 1758 s for **1** vs 1789 s, 1736 s cm^{-1} (THF) for **6**) and separation of NO stretching frequencies ($\Delta\nu_{NO} = 28$ cm^{-1} for **1** vs 53 cm^{-1} for **6**). Surprisingly, the formation of complex **5** was not observed upon addition of 2 equiv of PPh_3 to the THF solution of complex **6**. Obviously, in addition to the π-acceptor character of PPh_3, the presence or absence of an Fe···Fe interaction and the different binding modes of the bridged thiolates also play important roles in determining the reaction pathway to form neutral $\{Fe(NO)_2\}^{10}$ complex **5** upon the reactions of **1** or **6** with PPh_3.

As shown in Scheme 1g, conversion of the neutral dimeric DNIC **6** into the anionic $\{Fe(NO)_2\}^9$, DNIC $[(N_3)_2Fe(NO)_2]^-$ (**7**), was observed by treating complex **6** with 4 equiv of $[N_3]^-$ in THF under N_2 atmosphere. Presumably, complex **7** was produced via the bridged-thiolate cleavage forming $[(N_3)(-SC_7H_4SN)Fe(NO)_2]^-$ and the subsequent ligand-displacement reaction of $[(N_3)(-SC_7H_4SN)Fe(NO)_2]^-$ and $[N_3]^-$, since the nucleophilic attack on the Fe–S antibonding LUMO orbital of RRE $[Fe_2(\mu\text{-}SR)_2(NO)_4]$ leading to splitting of the thiolate bridges and formation of the anionic dinitrosyl iron complexes had been proposed.[13] Complex **7** was alternatively obtained via a ligand-displacement reaction between the anionic $\{Fe(NO)_2\}^9$, $[(-SC_7H_4SN)_2Fe(NO)_2]^-$, and 2 equiv of $[N_3]^-$ in THF (Scheme 1h,i). This result shows that the $[N_3]^-$-coordinated ligands of complex **7** promotes the stability of the $\{Fe(NO)_2\}^9$ DNICs compared to the anionic thiolate-coordinated ligands. Compared to the well-resolved nine-line and five-line EPR spectrum of complexes $[(SC_6H_4\text{-}o\text{-}NHCOPh)(Imidazole)Fe(NO)_2]$ and $[(SC_6H_4\text{-}o\text{-}NHCOPh)_2Fe(NO)_2]^-$ with a signal at $g = 2.031$ and 2.029, respectively,[7c] complex **7** exhibits an isotropic signal with $g = 2.027$ at 298 K and high rhombicities with three principal

(12) (a) Solomon, E. I. *Pure Appl. Chem.* **1983**, *55*, 1069–1088. (b) Rakova, O. A.; Sanina, N. A.; Aldoshin, S. M.; Goncharova, N. V.; Shilov, G. V.; Shulga, Y. M.; Ovanesyan, N. S. *Inorg. Chem. Commun.* **2003**, *6*, 145–148.

(13) (a) Jo, D.-H.; Chiou, Y.-M.; Que, L., Jr. *Inorg. Chem.* **2001**, *40*, 3181–3190. (b) Jaworska, M.; Stasicka, Z. *New J. Chem.* **2005**, *29*, 604–612. (c) Glidewell, C.; Johnson, I. L. *Polyhedron* **1988**, *7*, 1371–1375.

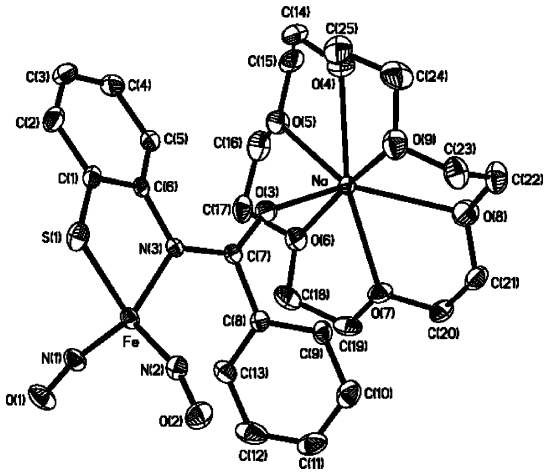

Figure 3. ORTEP drawing and labeling scheme of [Na-18-crown-6-ether]-[$(NO)_2Fe(SC_6H_4$-*o*-NC(O)Ph)] (**3**) with thermal ellipsoids drawn at 30% probability. Selected bond distances (Å) and angles (deg): Fe−N(1) 1.679(3); Fe−N(2) 1.688(3); Fe−N(3) 1.996(3); Fe−S(1) 2.2819(10); O(1)−N(1) 1.176(4); O(2)−N(2) 1.170(4); Na−O(3) 2.273(3); N(1)−Fe−N(2) 114.11(15); N(1)−Fe−N(3) 113.53(13); N(2)−Fe−N(3) 118.44(13); N(1)−Fe−S(1) 111.01(12); N(2)−Fe−S(1) 108.54(11); N(3)−Fe−S(1) 87.93(8); O(1)−N(1)−Fe 168.4(3); O(2)−N(2)−Fe 162.7(3).

g values of 2.043, 2.023, and 2.012 at 77 K (Supporting Information Figure S3).

Structures. The structure of the $[(SC_6H_4$-*o*-NCOPh)Fe-$(NO)_2]^-$ unit in the [Na-18-crown-6-ether]$^+$ salt is shown in Figure 3. The geometry about iron is a distorted tetrahedral with the bite angle of the chelating $[SC_6H_4$-*o*-NCOPh]$^{2-}$ ligand of 87.93(8)°. The five-membered chelate ring $FeSC_2N$ is almost planar, with a deviation from planarity of 32.4°. The shorter Fe−N(3) bond length (1.996(3) Å) in complex **3**, as compared to the reported 2.021(4) Å in $[(SC_6H_4$-*o*-NHCOPh)(imidazole)Fe$(NO)_2]$,[7c] was attributed to the π-donating ability of the bidentate $[SC_6H_4$-*o*-NCOPh]$^{2-}$ ligand which stabilizes the $\{Fe(NO)_2\}^9$ complex **3**. The Fe−N(1)-(O) and Fe−N(2)(O) bond lengths of 1.679(3) and 1.688(3) Å, respectively, also fall in the range 1.661(4)−1.695(3) Å observed in the anionic $\{Fe(NO)_2\}^9$ DNICs.[7d]

Figure 4 displays an ORTEP plot of the anionic mononuclear complex **4**, and the selected bond distances and angles are listed in the figure caption. The constraint of the $[SC_6H_4$-*o*-COO]$^{2-}$ ligand generates ca. 95.77(6)° O(3)−Fe−S(1) angle, enforcing a severe distortion from tetrahedral at the four-coordinated iron site. The nearly identical N(1)−O(1) and N(2)−O(2) bond lengths of 1.166(3) and 1.172(3) Å, respectively, are within the range (1.160(6)−1.178(3) Å) observed for the anionic $\{Fe(NO)_2\}^9$ DNICs,[7d] athough the Fe−N(1)(O) and Fe−N(2)(O) bond lengths of 1.677(2) and 1.691(2) Å, respectively, also fall in the range 1.661(4)−1.695(3) Å observed in the anionic $\{Fe(NO)_2\}^9$ DNICs.[7d] It is noticed that the Fe−N(1)−O(1) bond angle of 167.2(2)° is significantly distinct from the Fe−N(2)−O(2) bond angle of 157.1(2)° in complex **4**.

Figures 5 and 6 show the thermal ellipsoid plots of the neutral dimeric complex **6** and the anionic complex **7**, and the selected bond distances and angles are given in the figures captions, respectively. Complex **6** possesses crystallographically imposed centrosymmetry. Two four-coordinated Fe

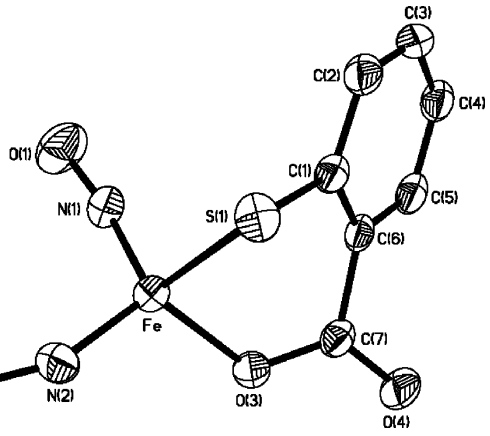

Figure 4. ORTEP drawing and labeling scheme of $[(NO)_2Fe(SC_6H_4$-*o*-COO)]$^-$ (**4**) with thermal ellipsoids drawn at 50% probability. Selected bond distances (Å) and angles (deg): Fe−N(1) 1.677(2); Fe−N(2) 1.691(2); Fe−O(3) 1.933(2); Fe−S(1) 2.2638(9); O(1)−N(1) 1.166(3); O(2)−N(2) 1.172-(3); N(1)−Fe−N(2) 111.20(12); N(1)−Fe−O(3) 114.55(11); N(2)−Fe−O(3) 114.19(11); N(1)−Fe−S(1) 107.32(9); N(2)−Fe−S(1) 112.72(9); O(3)−Fe−S(1) 95.77(6); O(1)−N(1)−Fe 167.2(2); O(2)−N(2)−Fe 157.1-(2).

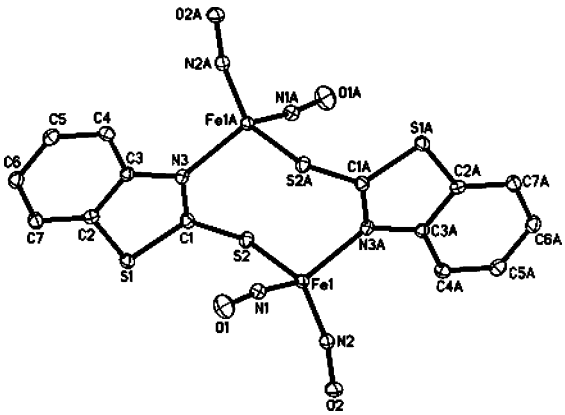

Figure 5. ORTEP drawing and labeling scheme of $[(\mu$-$SC_7H_4SN)Fe-(NO)_2]_2$ (**6**) with thermal ellipsoids drawn at 30% probability. Selected bond distances (Å) and angles (deg): Fe(1)−N(1) 1.6840(18); Fe(1)−N(2) 1.6897(18); Fe(1)−N(3A) 2.0459(17); Fe(1)−S(2) 2.2904(6); O(2)−N(2) 1.174(2); O(1)−N(1) 1.162(2); N(1)−Fe(1)−N(2) 113.35(8); N(1)−Fe(1)−N(3A) 114.39(8); N(2)−Fe(1)−N(3A) 109.67(7); N(1)−Fe(1)−S(2) 104.05-(6); N(2)−Fe(1)−S(2) 107.22(6); N(A)−Fe(1)−S(2) 107.60(5); O(2)−N(2)−Fe(1) 161.21(16); O(1)−N(1)−Fe(1) 167.37(17).

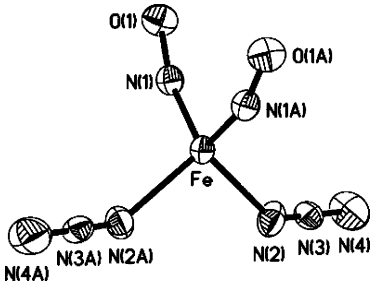

Figure 6. ORTEP drawing and labeling scheme of $[(N_3)Fe(NO)_2]^-$ (**7**) with thermal ellipsoids drawn at 30% probability. Selected bond distances (Å) and angles (deg): Fe−N(1) 1.694(2); Fe−N(2) 1.948(2); N(1)−O(1) 1.172(3); N(3)−N(4) 1.07(3); N(2)−N(3) 1.16(2); N(1A)−Fe−N(1) 108.53-(15); N(1A)−Fe−N(2) 114.14(10); N(1)−Fe−N(2) 109.09(11); O(1)−N(1)−Fe 160.7(2); N(2)−Fe−N(2A) 101.88(17); N(4)−N(3)−N(2) 174.2-(19).

atoms are connected via two $[-SC_7H_4SN-]^-$ bridges, and two pairs of NO groups (N(1)O(1), N(1A)O(1A) and N(2)O-(2), N(2A)O(2A)) point in the antiparallel direction. The

geometry of Fe(1) and Fe(1A) of complex **6** is consistent with the nearly regular tetrahedron. The long Fe···Fe distance of 3.997 Å resulting in the weak dipolar coupling between two $\{Fe(NO)_2\}^9$ centers may account for the paramagnetism and the EPR-active signal ($g = 2.033$ at 298 K) in complex **6**.[9] The Fe(1)−N(3A) bond length of 2.046(2) Å in complex **6** is longer than the Fe−N(imidazole) bond distance (2.021(4) Å) found in the neutral $\{Fe(NO)_2\}^9$, $[(SC_6H_4$-*o*-NHCOPh)(imidazole)$Fe(NO)_2]$.[7c]

Interestingly, complex **7** possesses crystallographically imposed centrosymmetry. The N−O bond distances of 1.172(7) Å in complex **7**, comparable to the average N−O bond distance of 1.169(3) Å observed in complex **4**, exactly fall in the range 1.178(3)−1.160(6) Å for the anionic $\{Fe(NO)_2\}^9$ DNICs,[7d] while the mean Fe−N(O) distances of 1.694(2) Å in complex **7** are nearly at the upper end of 1.695(3)−1.661(4) Å for the anionic $\{Fe(NO)_2\}^9$ DNICs.[7d] The significantly shorter Fe−N(2) bond length of 1.948(2) Å in complex **7**, as compared with the Fe−N(3) bond length of 1.996(3) Å in complex **3**, probably originates from the additional π-donating interactions of the N(2) and N(2A) with the Fe metal center.

Conclusion and Comments. Studies on the anionic $\{Fe(NO)_2\}^9$ DNICs with S/N/O ligation, the dimeric DNICs containing two separate $\{Fe(NO)_2\}^9$ dinitrosyl iron motifs, and the interconversion between the neutral $\{Fe(NO)_2\}^{10}$ $[L_2Fe(NO)_2]$ (L = the neutral P-containing ligand) and the Roussin's red ester $[(NO)_2Fe(\mu\text{-}SR)_2Fe(NO)_2]$ have led to the following results, including certain results from earlier studies.[7,9]

(1) The weaker σ-donating, neutral imidazole triggers the bridged-thiolate cleavage of RRE **1** to yield the neutral $\{Fe(NO)_2\}^9$, $[(SC_6H_4$-*o*-NHCOPh)(Im)$Fe(NO)_2]$ (Im = imidazole), when complex **1** was reacted with 2 equiv of imidazole.[7c] In contrast, the stronger σ-donating and π-accepting PPh_3 ligand induces the reductive elimination of bridged thiolates of RRE **1** to yield the neutral $\{Fe(NO)_2\}^{10}$, $[(PPh_3)_2Fe(NO)_2]$. However, the reaction of complex **1** and $[OPh]^-$ triggers deprotonation of complex **1** to yield complex **3**. The above results unambiguously illustrate one aspect of how nucleophile L (L = imidazole, $[OPh]^-$, PPh_3) functions to modulate the reaction pathways (bridged-thiolate cleavage, deprotonation, and reductive elimination) to yield the neutral/anionic $\{Fe(NO)_2\}^9$ and the neutral $\{Fe(NO)_2\}^{10}$ DNICs upon the reaction of complex **1** and nucleophile L.

(2) The EPR-active $\{Fe(NO)_2\}^9$ DNICs can be grouped into (i) the anionic $\{Fe(NO)_2\}^9$ DNICs with S/N/O ligation (types I−IV, as shown in the following graphic), (ii) the neutral $\{Fe(NO)_2\}^9$ DNIC with one thiolate and one neutral imidazole ligation (type V, shown in the following graphic),[7c] and (iii) the cationic $\{Fe(NO)_2\}^9$ DNIC with the neutral N-/P-containing ligands (type VI, shown in the following graphic).[7d,14]

(3) The π-acceptor character of the nucleophile L, the dimeric DNICs **1**/**6** with/without Fe···Fe coupling and the

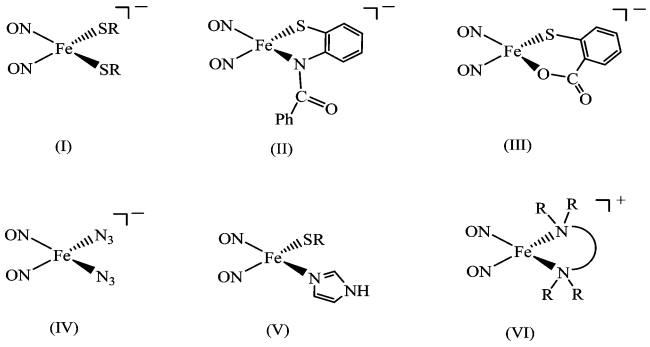

different bonding modes of the bridged thiolates of DNICs **1**/**6** may play the role to determine the reaction pathway to form the neutral $\{Fe(NO)_2\}^{10}/\{Fe(NO)_2\}^9$ DNICs upon the reaction of complexes **1**/**6** and nucleophile L.[7c,7d]

(4) The dimeric DNICs can be classified into three different types: (i) the EPR-silent DNICs (Roussin's red ester) with two $\{Fe(NO)_2\}^9$ dinitrosyl iron motifs stabilized by $\{Fe(NO)_2\}^9-\{Fe(NO)_2\}^9$ coupling (Fe···Fe ≈ 2.5−2.6 Å; type I, shown in the following graphic);[6,11] (ii) the EPR-active, dimeric DNICs containing two separate, neutral $\{Fe(NO)_2\}^9$ dinitrosyl iron motifs (Fe···Fe distance of 4.0 Å, type II, shown in the following graphic);[12] (iii) the EPR-silent, dinuclear DNICs with one $\{Fe(NO)_2\}^9$ dinitrosyl iron motif stabilized by $\{Fe(NO)\}^7-\{Fe(NO)_2\}^9$ coupling (Fe···Fe distance of 2.66 Å, type III, shown in the following graphic).[9]

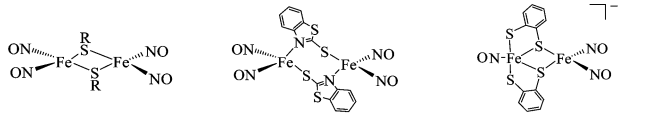

$\{Fe(NO)_2\}^9$-$\{Fe(NO)_2\}^9$ Fe···Fe ≈ 2.5~2.6 Å (I)

$\{Fe(NO)_2\}^9$···$\{Fe(NO)_2\}^9$ Fe···Fe ≈ 4.0 Å (II)

$\{Fe(NO)_2\}^7$-$\{Fe(NO)_2\}^9$ Fe···Fe ≈ 2.66 Å (III)

(5) The facile interconversion between the neutral $\{Fe(NO)_2\}^{10}$, $[L_2Fe(NO)_2]$ (L = the neutral N-/P-containing ligand), and the anionic $\{Fe(NO)_2\}^9$, $[(RS)_2Fe(NO)_2]^-$, was demonstrated, as shown in Scheme 2. The transformation of the neutral $\{Fe(NO)_2\}^{10}$ DNICs **A** to the anionic $\{Fe(NO)_2\}^9$ DNICs **C** may occur via the cationic $\{Fe(NO)_2\}^9$ DNICs **B** (Scheme 2a,b).[7d,14] Transformation of the anionic $\{Fe(NO)_2\}^9$ DNICs **C** to the neutral $\{Fe(NO)_2\}^{10}$ DNICs **A** may occur through the formation of the Roussin's red ester **D** followed by the neutral ligand L (=PPh_3) triggering the reductive elimination of the bridged thiolates, as observed in this study (Scheme 2c,d).

Experimental Section

Manipulations, reactions, and transfers were conducted under nitrogen according to Schlenk techniques or in a glovebox (argon gas). Solvents were distilled under nitrogen from appropriate drying agents (acetonitrile from $CaH_2-P_2O_5$; methylene chloride from CaH_2; diethyl ether, hexane, and tetrahydrofuran (THF) from sodium benzophenone) and stored in dried, N_2-filled flasks over 4 Å molecular sieves. Nitrogen was purged through these solvents before use. Solvent was transferred to the reaction vessel via

(14) Atkinson, F. L.; Blackwell, H. E.; Brown, N. C.; Connelly, N. G.; Crossley, J. G.; Orpen, A. G.; Rieger, A. L.; Rieger, P. H. *J. Chem. Soc., Dalton Trans.* **1996**, 3491−3502.

Scheme 2

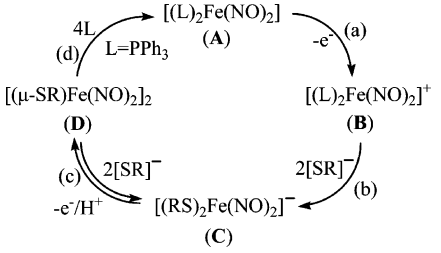

stainless cannula under positive pressure of N_2. The reagents iron pentacarbonyl, sodium nitrite, bis(2-benzothiozolyl) disulfide, bis(triphenylphosphoranylidene)ammonium chloride ([PPN][Cl]) (Aldrich), sodium azide, bis(*o*-benzamidophenyl) disulfide, 2,2′-dithiodibenzoic acid, 18-crown-6-ether (TCI), and sodium phenoxide (Alfa Aesar) were used as received. Compounds $(CO)_2Fe(NO)_2$ and $(Ph_3P)_2Fe(NO)_2$ were synthesized by published procedures.[10] Infrared spectra of the ν(NO) and ν(COO) stretching frequencies were recorded on a Perkin-Elmer model spectrum one B spectrophotometer with sealed solution cells (0.1 mm, KBr windows) or KBr solid. UV−vis spectra were recorded on a GBC Cintra 10e and Jasco V-570. ^{1}H spectra were obtained on a Varian Unity-500 spectrometer. Analyses of carbon, hydrogen, and nitrogen were obtained with a CHN analyzer (Heraeus).

Preparation of [Fe(μ-SC_6H_4-*o*-NHC(O)Ph)$(NO)_2]_2$ (1). The THF solution (5 mL) of $Fe(CO)_2(NO)_2$ (0.4 mmol) freshly prepared was added to the THF (4 mL) solution of bis(*o*-benzamidophenyl) disulfide (0.2 mmol, 0.091 g) by cannula under a positive N_2 pressure at 0 °C. The resulting solution was stirred at ambient temperature overnight. The solution was filtered through Celite, and hexane was then added to precipitate the brown-green solid [Fe(μ-SC_6H_4-*o*-NHC(O)Ph)$(NO)_2]_2$ (**1**) (yield 0.124 g, 90%) characterized by ^{1}H NMR, IR, and UV−vis spectra.[5a,11a] IR ν_{NO}: 1758 s, 1786 s, 1816 vw (THF) cm^{-1}. Absorption spectrum (CH_2Cl_2) [λ_{max}, nm (ϵ, M^{-1} cm^{-1})]: 373 (6152), 438 (6104), 780 (120). ^{1}H NMR (CD_2Cl_2): δ 9.04 (br), 8.98 (br) (N−H), 8.45−6.55 (m) (S, N−C_6H_4, −C_6H_5) ppm.

Preparation of [Fe(μ-SC_6H_4-*o*-COOH)$(NO)_2]_2$ (2). Compound 2,2′-dithiodibenzoic acid (0.2 mmol, 0.061 g) was dissolved in THF (4 mL) in the 25 mL Schlenk flask, and THF solution (5 mL) of $Fe(CO)_2(NO)_2$ (0.4 mmol) freshly prepared was added to it by cannula under a positive N_2 pressure at 0 °C. The resulting solution was stirred at ambient temperature overnight. Solvent was then removed under vacuum. The crude solid was redissolved in THF and then filtered through Celite. Addition of hexane to the brown filtrate led to the precipitation of brown solid [Fe(μ-SC_6H_4-*o*-COOH)$(NO)_2]_2$ (**2**) (yield 0.19 g, 66%) characterized by ^{1}H NMR, IR, and UV−vis spectra.[7c] IR ν_{NO}: 1756 s, 1782 s, 1812 vw (THF) cm^{-1}. Absorption spectrum (THF) [λ_{max}, nm (ϵ, M^{-1} cm^{-1})]: 387 (12413), 662 (694), 792 (353). ^{1}H NMR (C_4D_8O): δ 6.92−8.08 (m) (C_6H_4), 10.58 (br) (COOH) ppm.

Preparation of [Na-18-crown-6-ether][$(NO)_2$Fe(SC_6H_4-*o*-NC(O)Ph)] (3). The THF solution (5 mL) of complex **1** (0.061 g, 0.2 mmol), sodium phenoxide (0.0464 g, 0.4 mmol), and 18-crown-6-ether (0.106 g, 0.4 mmol) was stirred under N_2 for 3 h at room temperature. The mixture solution was filtered through Celite, and hexane was then added to precipitate the black-purple solid [Na-18-crown-6-ether][$(NO)_2$Fe(SC_6H_4-*o*-NC(O)Ph)] (**3**) (0.16 g, 63%). X-ray quality crystals were obtained by diffusion of diethyl ether−hexane (1:1 volume ratio) into THF solution of complex **3** at −20 °C for three weeks. IR ν_{NO}: 1690 s, 1737 s (THF) cm^{-1}. Absorption spectrum (THF) [λ_{max}, nm (ϵ, M^{-1} cm^{-1})]: 455 (3803), 560 (3415), 667 (1965). Anal. Calcd for $C_{25}H_{33}O_9SN_3FeNa$: C, 47.63; H, 5.28; N, 6.67. Found: C, 47.51; H, 6.04; N, 6.79.

Preparation of [PPN][$(NO)_2$Fe(SC_6H_4-*o*-COO)] (4). The THF solution (5 mL) of complex **2** (0.1112 g, 0.2 mmol) and sodium phenoxide (0.0464 g, 0.4 mmol) was stirred at ambient temperature for 30 min. The resulting solution was then transferred to a 50 mL Schlenk flask containing 0.230 g of [PPN][Cl] (0.4 mmol), and the mixture solution was stirred overnight at ambient temperature. The mixture solution was filtered through Celite to remove NaCl, and solvent was then removed under vacuum to obtain the dark-brown solid [PPN][$(NO)_2$Fe(SC_6H_4-*o*-COO)] (**4**) (0.126 g, 78%). Diffusion of hexane into THF solution of complex **4** at −20 °C for four weeks led to the dark-brown crystals suitable for X-ray crystallography. IR: 1688 s, 1742 s (ν_{NO}); 1625 s (ν_{CO}) (THF) cm^{-1}. Absorption spectrum (THF) [λ_{max}, nm (ϵ, M^{-1} cm^{-1})]: 426 (1775), 475 (1420), 670 (424), 947 (123). Anal. Calcd for $C_{43}H_{34}O_4SN_3P_2Fe$: C, 64.03; H, 4.25; N, 5.21. Found: C, 63.93; H, 4.50; N, 5.12.

Reaction of [Fe(μ-SC_6H_4-*o*-NHC(O)Ph)$(NO)_2]_2$ (1) and PPh_3. The THF solution of complex **1** (0.2 mmol), freshly prepared from reaction of $[Fe(CO)_2(NO)_2]$ (0.4 mmol) and bis(*o*-benzamidophenyl) disulfide (0.2 mmol, 0.091 g) in THF (5 mL), was transferred to a 50-mL Schlenk flask loaded with PPh_3 (0.105 g, 0.8 mmol) by a cannula under positive N_2 pressure at ambient temperature. The mixture solution was stirred for 1 h. The solution was then concentrated, and diethyl ether−hexane (5:15 mL) was added to precipitate yellow-brown solid $[(PPh_3)_2Fe(NO)_2]$ (**5**). The resulting mixture was then filtered to separate the solid and solution. The yellow-brown solid was redissolved in THF, and then diffusion of hexane into the THF solution of complex **5** at −15 °C led to the brown crystals of the known complex **5** (yield 0.236 g, 92%) identified by IR (IR ν_{NO}: 1676 s, 1718 s cm^{-1} (THF)), UV−vis (absorption spectrum (THF) [λ_{max}, nm]: 445, 665),[10b,c] and single-crystal X-ray diffraction. The THF−diethyl ether−hexane filtrate was dried under vacuum to acquire the greenish-yellow solid, and then diethyl ether was added to extract bis(*o*-benzamidophenyl) disulfide characterized by ^{1}H NMR (^{1}H NMR ($CDCl_3$): δ 6.92 (t), 7.27 (t), 7.41 (m), 7.53 (t), 7.66 (d), 8.47 (d) (Ph); 8.91 (br) (NH) ppm).

Preparation of [Fe(μ-$SC_7H_4SN)(NO)_2]_2$ (6). Bis(2-benzothiozolyl) disulfide (0.033 g, 0.1 mmol) was added into the THF solution of $[Fe(CO)_2(NO)_2]$, freshly prepared from reaction of [PPN]-$[Fe(CO)_3NO]$ (0.141 g, 0.2 mmol) and $[NO][BF_4]$ (0.024 g, 0.2 mmol), and stirred for 30 min under N_2 atmosphere at ambient temperature. The reaction was monitored with FTIR. IR spectrum (IR ν_{NO}: 1736 s, 1789 s cm^{-1} (THF)) was assigned to the formation of [Fe(μ-$SC_7H_4SN)(NO)_2]_2$ (**6**). Diffusion of hexane into the THF solution of complex **6** at −15 °C led to the dark red crystals suitable for single-crystal X-ray diffraction (yield 0.050 g, 89%). IR ν_{NO}: 1736 s, 1789 s cm^{-1} (THF). Absorption spectrum (THF) [$\lambda_{max,}$ nm (ϵ, M^{-1} cm^{-1})]: 428 (984), 549 (241), 753(55). Anal. Calcd for $C_{14}H_8N_6O_4S_4Fe$: C, 29.80; H, 1.43; N, 14.90. Found: C, 30.21; H, 1.55; N, 15.26.

Reaction of $[(PPh_3)_2Fe(NO)_2]$ (5) and Bis(2-benzothiozolyl) Disulfide. A THF solution (10 mL) of $[(PPh_3)_2Fe(NO)_2]$ (0.128 g, 0.2 mmol) was transferred to a 50 mL Schlenk flask loaded with bis(2-benzothiozolyl) disulfide (0.033 g 0.1 mmol) by cannula under positive N_2 pressure at room temperature. The reaction mixture was stirred for 2 h at room temperature. The solution was concentrated under vacuum, and hexane was added to precipitate the dark-red solid assigned to the formation of complex **6** (yield 0.047 g, 83%) characterized by IR (IR ν_{NO}: 1736 s, 1789 s cm^{-1} (THF)), and UV−vis (absorption spectrum (THF) [$\lambda_{max,}$ nm]: 428, 549, 753).

Reaction of [Fe(μ-SC_7H_4SN-)$(NO)_2]_2$ (6) and [PPN][SC_7H_4SN]. Complex **6** (0.113 g, 0.2 mmol) and [PPN][SC_7H_4SN] (0.282 g, 0.4 mmol) were dissolved in THF (20 mL) under N_2 atmosphere. The reaction mixture was stirred at room temperature for 1 h, and then diethyl ether was added to precipitate the dark-red solid [PPN][$(SC_7H_4SN)_2Fe(NO)_2$] (**8**) (yield 0.371 g, 94%) characterized by IR (IR ν_{NO}: 1716 s, 1766 s cm^{-1} (THF)), and UV−vis (absorption spectrum (THF) [λ_{max}, nm]: 465, 799 nm).[7b]

Preparation of [PPN][$(N_3)_2Fe(NO)_2$] (7). Complex **6** (0.0524 g, 0.1 mmol) and [PPN][N_3] (0.232 g, 0.4 mmol) were dissolved in THF (20 mL) under N_2 atmosphere. The reaction mixture was stirred at room temperature overnight, and the resulting solution was filtered through Celite to separate the insoluble solid. The reaction solution was monitored with FTIR. IR spectrum (ν_{NO}: 1698 s, 1755 s cm^{-1} (THF)) was assigned to the formation of [PPN][$(N_3)_2Fe(NO)_2$] (**7**). Diffusion of hexane into the THF solution of complex **7** at −15 °C led to the red-brown crystals suitable for single-crystal X-ray diffraction (yield 0.129 g, 87%). IR ν_{NO}: 1698 s, 1755 s cm^{-1} (THF). Absorption spectrum (THF) [λ_{max}, nm (ϵ, M^{-1} cm^{-1})]: 397 (6163), 502 (829), 701 (356). Anal. Calcd for $C_{36}H_{30}N_9P_2O_2Fe$: C, 58.55; H, 4.09; N, 17.07. Found: C, 58.18; H, 4.73; N, 16.91.

Reaction of [PPN][$(SC_7H_4SN)_2Fe(NO)_2$] and [PPN][N_3]. A THF solution (15 mL) of complex **8** (0.392 g, 0.4 mmol) was transferred to a 50 mL Schlenk flask loaded with [PPN][N_3] (0.464 g, 0.8 mmol) by a cannula under positive N_2 pressure at room temperature. The reaction solution was stirred overnight at room temperature, and the resulting mixture was filtered through Celite to separate the insoluble solid. The solution was then concentrated under vacuum, and diethyl ether−hexane (15:15 mL) was added to precipitate the red-brown solid complex **7** (yield 0.230 g, 78%) characterized by IR (IR ν_{NO}: 1698 s, 1755 s cm^{-1} (THF)) and UV−vis (absorption spectrum (THF) [λ_{max}, nm (ϵ, M^{-1} cm^{-1})]: 397, 502, 701 nm).

EPR Measurements. EPR measurements were performed at X-band using a Bruker EMX spectrometer equipped with a Bruker TE102 cavity. The microwave frequency was measured with a Hewlett-Packard 5246L electronic counter. X-band EPR spectra of complexes **3**, **4**, **6**, and **7** in THF were obtained with a microwave power of 15.902, 20.020, 7.970, and 6.331 mW, frequency at 9.603, 9.600, 9.595, and 9.598 GHz, respectively, and modulation amplitude of 0.80 G (1.6 G for complex **4**) at 100 kHz. The specific temperatures of EPR measurements for complexes **3**, **4**, **6**, and **7** were controlled by the helium temperature controller (3.8−300 K; Bruker EMX model).

Magnetic Measurements. The magnetization data were recorded on a SQUID magnetometer (MPMS5 Quantum Design Company) with an external 0.5 (or 1) T magnetic field in the temperature range 2−300 K. The magnetic susceptibility of the experimental data was corrected for diamagnetism by the tabulated Pascal's constants.

Crystallography. Crystallographic data and structure refinements parameters of complexes **2**, **3**, **6**, and **7** are summarized in the Supporting Information. The crystals chosen for X-ray diffraction studies measured 0.40 × 0.25 × 0.25 mm^3 for complex **2**, 0.27 × 0.25 × 0.20 mm^3 for complex **3**, 0.30 × 0.20 × 0.05 mm^3 for complex **6**, and 0.25 × 0.25 × 0.20 mm^3 for complex **7**, respectively. Each crystal was mounted on a glass fiber and quickly coated in epoxy resin. Unit-cell parameters were obtained by least-squares refinement. Diffraction measurements for complexes **2**, **3**, **6**, and **7** were carried out on a SMART Apex CCD diffractometer with graphite-monochromated Mo Kα radiation (λ = 0.7107 Å) and between 2.24° and 27.50° for complex **2**, between 1.42° and 27.50° for complex **3**, between 2.51° and 28.33° for complex **6**, and between 1.94° and 27.49° for complex **7**. Least-squares refinement of the positional and anisotropic thermal parameters of all non-hydrogen atoms and fixed hydrogen atoms was based on F^2. A SADABS[15] absorption correction was made. The SHELXTL[16] structure refinement program was employed.

Acknowledgment. We gratefully acknowledge financial support from the National Science Council of Taiwan. Authors thank Mr. Mu-Cheng Hung for compilation of Table 1, and Miss Chun-Yu Chen for single-crystal X-ray structure determinations.

Supporting Information Available: X-ray crystallographic files in CIF format for the structure determinations of [(μ-SC_7H_4SN)-$Fe(NO)_2]_2$, [PPN][$(NO)_2Fe(SC_6H_4$-*o*-COO)], [Na-18-crown-6-ether]-[$(NO)_2Fe(SC_6H_4$-*o*-NC(O)Ph)], and [PPN][$(N_3)Fe(NO)_2$]. This material is available free of charge via the Internet at http://pubs.acs.org.

IC0702567

(15) Sheldrick, G. M. *SADABS, Siemens Area Detector Absorption Correction Program*; University of Göttingen: Göttingen, Germany, 1996.
(16) Sheldrick, G. M. *SHELXTL, Program for Crystal Structure Determination*; Siemens Analytical X-ray Instruments Inc.: Madison, WI, 1994.